Two-Photon Confocal Microscopy: A Nondestructive Method for Studying Wound Healing

Fernando A. Navarro, M.D., Peter T. C. So, Ph.D., Rubin Nirmalan, M.D., Nina Kropf, M.D., Farrant Sakaguchi, S.B., Christine S. Park, M.D., Hoon B. Lee, M.D., and Dennis P. Orgill, M.D., Ph.D.

Boston and Cambridge, Mass.

Two-photon confocal microscopy is a new technology useful in nondestructive analysis of tissue. The pattern generated from laser-excited autofluorescence and second harmonic signals can be analyzed to construct a three-dimensional, microanatomical, structural image. The healing of full-thickness guinea pig skin wounds was studied over a period of 28 days using two-photon confocal microscopy. Three-dimensional data were rendered from two-dimensional images and compared with conventional, en face, histologic sections. Two-photon confocal microscopy images show resolution of muscle, fascia fibers, collagen fibers, inflammatory cells, blood vessels, and hair. Although these images do not currently have the resolution of standard histology, the ability to noninvasively acquire three-dimensional images of skin promises to be an important tool in wound-healing studies. (*Plast. Reconstr. Surg.* 114: 121, 2004.)

Advances in histopathology and immunohistochemistry allow for the precise and detailed imaging of microanatomical tissues, but much of the cellular biochemical information is inevitably lost during the surgical and fixation processes. Two-photon confocal microscopy is a new technology useful in nondestructive analysis of tissue.

Two-photon confocal microscopy uses a technology similar to laser scanning confocal microscopy. Laser scanning confocal microscopy focuses a small spot of light on a fluorescent specimen. The emitted fluorescent light is analyzed while scanning the specimen to produce anatomic data. Two-photon confocal microscopy (TPCM) offers several advantages over single-photon microscopy (laser scanning confocal microscopy). Two-photon excitation uses near infrared photons, which penetrate farther into tissue than potentially damaging, shorter wavelength photons (i.e., photons used in single-photon microscopy). This allows visualization of deeper structures with less risk of tissue photodamage. Because two-photon excitation is quadratically related to the illumination intensity at the focal point, there is very little background emission and photodamage; only at the focal point is there a significant concentration of photons. Two-photon microscopy also has the inherent benefit of optical sectioning, allowing the construction of three-dimensional images of scanned structures.

Two-photon excitation occurs by the nearly simultaneous absorption of two photons by a molecule normally excitable by one photon of twice the energy. For example, the absorption either of a single 400-nm photon or of two 800-nm photons excites the same chromophore. In other words, either absorption pattern leads to the same electron transition, which fluoresces at a distinct wavelength. Our studies involve fluorescence of near-ultraviolet wavelengths. A high spatial concentration of photons at the imaged point is necessary for two-photon excitation. The proper concentration is achieved by use of a high-numerical-aperture objective while focusing a high-peak-power laser on a diffraction-limited spot. The laser's peak power is further increased by using a femtosecond laser source, which intensifies the laser light by rapid pulsing. The resultant peak excitation intensities are 10^6 times greater than the typical peak intensities used in laser

From the Division of Plastic Surgery, Brigham and Women's Hospital; the Tissue Engineering and Wound Healing Laboratory, Harvard Medical School; and the Massachusetts Institute of Technology. Received for publication May 2, 2003; revised September 19, 2003.

DOI: 10.1097/01.PRS.0000128374.20913.4B

scanning confocal microscopy. The fluorescence emission increases quadratically with the excitation intensity.

The two-photon technique uses conventional visible light optics in both scanning (excitation) and imaging (emission) components, because both excitation and emission wavelengths (~700 nm and ~400 nm) are within the visible spectrum. Different chromophores emit different wavelength when excited, allowing for the identification of different chemicals within the sample. The fluorescence from NAD(P)H can be used as an indicator of cellular redox metabolism.[1] NAD(P)H fluorescence is normally excited with light of approximately 360 nm and emits in the spectrum of 400 to 500 nm. The fluorescence of the reduced form, NAD(P)H, is significantly greater than it is for the oxidized form, NAD(P); therefore, fluorescence intensity can be used to monitor cellular hypoxia; however, care must be taken, because of possible interactions with other molecules such as elastin. Flavoproteins are excited at approximately 450 nm and fluoresce between 500 and 600 nm. The crosslinks in elastin are excited by wavelengths between 340 and 370 nm and have an emission of 400 to 450 nm.[2–4] Although collagen and tropocollagen crosslinks are autofluorescent with excitation in the range of 280 to 320 nm, fluorescence from collagen is not readily excited by a titanium:sapphire-based light source (Fig. 1). However, collagen can be readily visualized on the basis of second harmonic generated signal.[5,6] The fluorescence emitted by the endogenous chromophores of the sample is collected and transmitted toward the photon detector. The collected photons are counted and the number is transmitted to the data acquisition computer.

The development of an in vivo microscope with the objective positioned along the *z*-axis was designed and constructed for the purpose of obtaining vertical optical sections across the thickness of the in vivo human cornea.[7] An earlier study described the use of two-photon confocal microscopy to visualize normal guinea pig skin.[8] The study presented in this article used the same microscope to obtain sequential images of full-thickness guinea pig skin wounds over a period of 28 days.

Materials and Methods

Two-Photon Confocal Microscope

The TPCM is located in the Department of Mechanical Engineering at the Massachusetts Institute of Technology. The design of this microscope is shown schematically in Figure 2, *above*. It consists of a titanium:sapphire laser (Mira 900, Coherent Inc., Palo Alto, Calif.), characterized by a high average power of 1.5 W, with a fixed wavelength of 780 nm, emitted in short, 150-fsec pulses at 80 MHz. The laser light is directed into the microscope by means of a computer controlled, x-y scanner (Cambridge Technology, Watertown, Mass.). These motor-driven mirrors control the imaging of each pixel within each transverse section. The scan and tube lenses are located along the epiluminescence light path. They function together as a beam expander, which overfills the back aperture of the objective lens. A dichroic mirror (Chroma Technology, Inc., Brattleboro, Vt.) is a short-pass filter. It reflects the excitation laser (infrared) to the objective (Zeiss Fluar 40×, aperture 1.3) but transmits the fluorescence (ultraviolet) emitted by the sample. The objective axial position is driven by a computer-interfaced piezo-electric device (PI, Inc., Auburn, Mass.) so that the photons focus at different depths within the tissue.

The ultraviolet emission follows the initial illumination path down through the objective

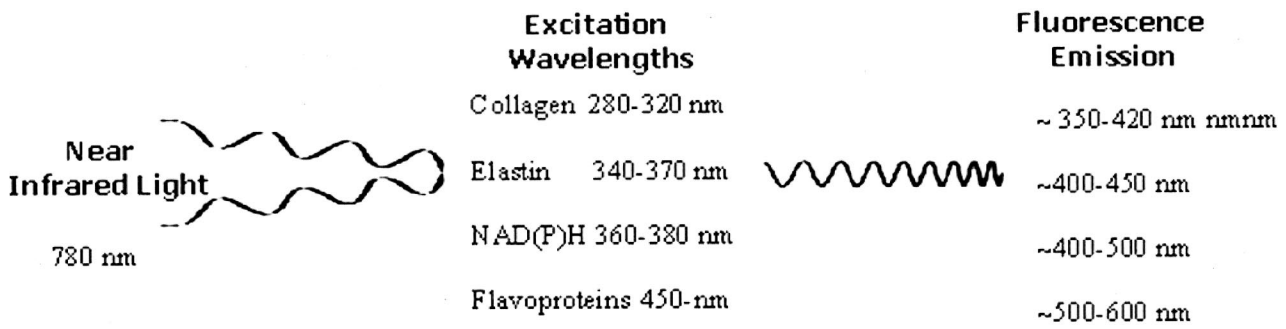

FIG. 1. Natural chromophore-specific wavelength emission after excitation by the absorption of two lower energy photons (infrared light).

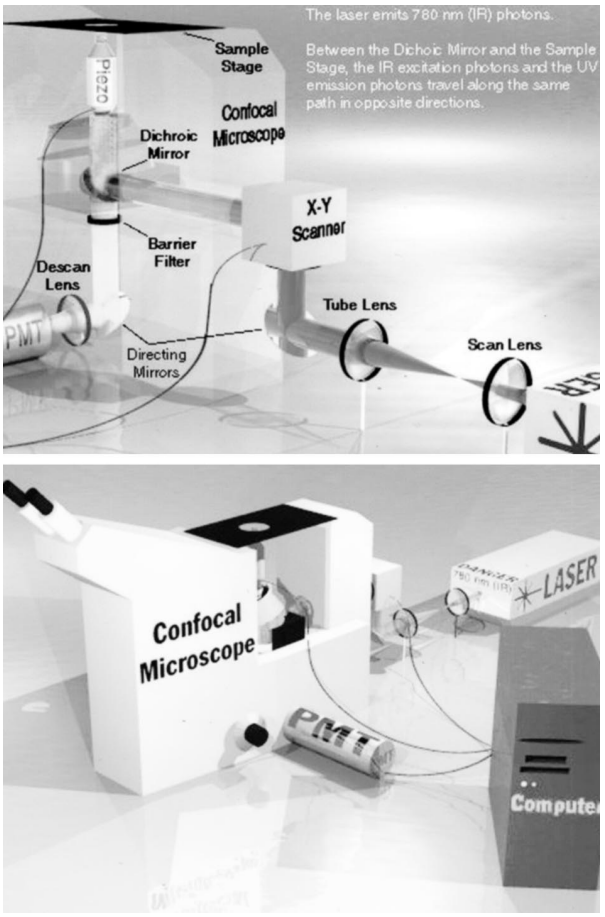

FIG. 2. (*Above*) Schematic representation of the two-photon deep tissue microscope. (*Below*) Schematic representation of the laser-microscope computer system. Images are visualized in three dimensions and animated using an interactive program.

and is transmitted by the dichroic mirror through a barrier filter (2 mm, BG39 Schott glass filter, Livermore, Calif.). The barrier filter eliminates most of the residual scatter with a minimum attenuation of the fluorescence. A descan lens collects the excitation, ensuring that the emission light strikes the photomultiplier tube (model R7400-P, Hamanatsu, Bridgewater, N.J.) at the same position. The photomultiplier tube is a single-photon counting module with a high quantum efficiency of 12 percent at 500 nm and 25 percent at 400 nm. A 100-MHz single-photon counting discriminator (F-100T, Advanced Research Instruments, Boulder, Colo.) converts single-photon bursts into digital pulses. Finally, the number of photons counted is transmitted to a data acquisition computer and the image stacks are visualized in three dimensions and animated using Spyglass Slicer (Fortner Research, Sterling, Va.), an interactive program (Fig. 2, *below*). Spyglass Slicer gives the user control over the creation and manipulation of slices, cubes, cutouts, image size and orientation, colors, shading, and transparency.

Animal Model

Animals were cared for in an Association for Assessment and Accreditation of Laboratory and Animal Care–accredited facility under an approved institutional protocol. The Institutional Committee for the Use of Animal Research has observed National Institutes of Health guidelines for the care and use of laboratory animals (National Institutes of Health publication 85-23, 1985 revision). Seven female Hartley guinea pigs weighing 400 to 475 g (Harlan Sprague-Dawley, Indianapolis, Ind.) were anesthetized with ketamine (10 mg/kg administered intramuscularly) and xylazine (2.2 mg/kg administered intramuscularly). Dorsal hair was clipped, treated with a chemical depilatory (Nair, Church & Dwight Co., Princeton, N.J.), shaved, and cleansed with germicide soap. A full-thickness skin wound, 1.5 × 1.5 cm, was created down to, but not including, the panniculus carnosus, using a scalpel. Hemostasis was obtained by direct pressure. The wound was dressed with Xeroform (Sherwood, St. Louis, Mo.), cotton gauze, and Elastoplast (Beiersdorf-Jobst, Rutherford College, N.C.). The dressing was changed on days 2 and 4 and removed on day 6.

Immediately before analysis (on days 0, 3, 7, 10, 14, 21, and 28), one animal was euthanized in a carbon dioxide chamber. The wound of the euthanized animal was subsequently analyzed by both TPCM and standard histologic methodology.

Approximately 40 TPCM images were obtained at 2.5-μm increments along the *z*-axis, to a depth of approximately 100 μm. Additional images were obtained after the wound bed was stained with cyto-20, a DNA stain. The typical image stacks had a lateral dimension of 117 × 117 μm and an axial dimension of 100 μm. Using Spyglass Slicer, the data obtained from the TPCM were analyzed and enhanced by subjectively adjusting the color table and the saturation of the images for maximal contrast.

Wounds and normal skin were excised immediately after imaging, stored in 10% formalin, embedded in paraffin, sectioned into 10-μm transverse and en face sections, and stained with hematoxylin and eosin. The slides were then visualized using a light microscope

at 40× magnification. As much as possible, we tried to compare similar areas of skin using TPCM and hematoxylin and eosin histologic sections, which we used as our standard.

Results

Constructed TPCM images were correlated with en face light microscopy sections stained with hematoxylin and eosin. TPCM images of the unwounded skin showed several readily identifiable structures; in the upper layers, a highly florescent stratum corneum followed by smaller cuboidal basal cells was seen.

Images of freshly excised skin wound (day 0) show an absolute lack of any dermal or epidermal structures. Fascia fibers were identified, and lobulated, less fluorescent structures consistent with muscle were visualized at 12.5 μm. These structures were similar to those seen on light microscopy, 10 μm deep (Fig. 3, *left* and *center*). The structures seen by light microscopy are typical of muscle cells, with characteristic peripheral nuclear distribution. Images of the DNA-stained wound reveal DNA activity at the center of the wound (Fig. 3, *right*).

TPCM images from day 3 show fascia fibers at 7.5 μm (Fig. 4, *above*, *left*) and an increase in the number of inflammatory cells embedded in the fibrin matrix (Fig. 4, *below*, *left*). Light microscopy of an en face section 7.5 μm deep into the wound bed shows disorganized fascia fibers (Fig. 4, *above*, *right*) and a marked increase in cellularity near the wound surface (Fig. 4, *below*, *right*). There appear to be more inflammatory cells in the hematoxylin and eosin than the TPCM. This may be a result of imaging slightly different tissue levels.

TPCM images at day 7, 12.5 μm deep, show a few new blood vessels. What had been early collagen fibers (or a collagen gel) now appear to be thicker, denser, and to have stronger second harmonic emissions. This was confirmed by comparing these images with their respective en face light microscopy sections at the same depth. The level of DNA activity in the superficial layers (~10 μm depth) was higher than in previous days.

At day 10, numerous new blood vessels and a thicker, denser population of collagen fibers is seen in the TPCM image 15 μm deep into the wound surface (Fig. 5, *left*). These findings are corroborated in the correlating light microscopy section, also 15 μm into the wound surface. Figure 5, *center*, shows capillary sprouts, some joined at their tips forming capillary loops. The level of DNA activity in the superficial layers was higher that that of previous days (Fig. 5, *right*).

Thicker and denser collagen fibers are more apparent in the TPCM images (Fig. 6, *left*) (17 μm deep from the wound surface) on day 14 than before. The en face microscopy sections show a connective tissue matrix deposition formed by fibroblasts, macrophages, and new blood vessels (Fig. 6, *right*), 17 μm deep into the surface of the wound biopsy specimen.

At day 21, epidermal cells are seen. A segment of the "epidermal tongue" has begun migrating toward the center of the wound. This consists mainly of smaller basal cells that are intensely fluorescent. The respective light microscopy section shows a migration of epithelial cells in a pseudopodia-like pattern into a fibronectin matrix.

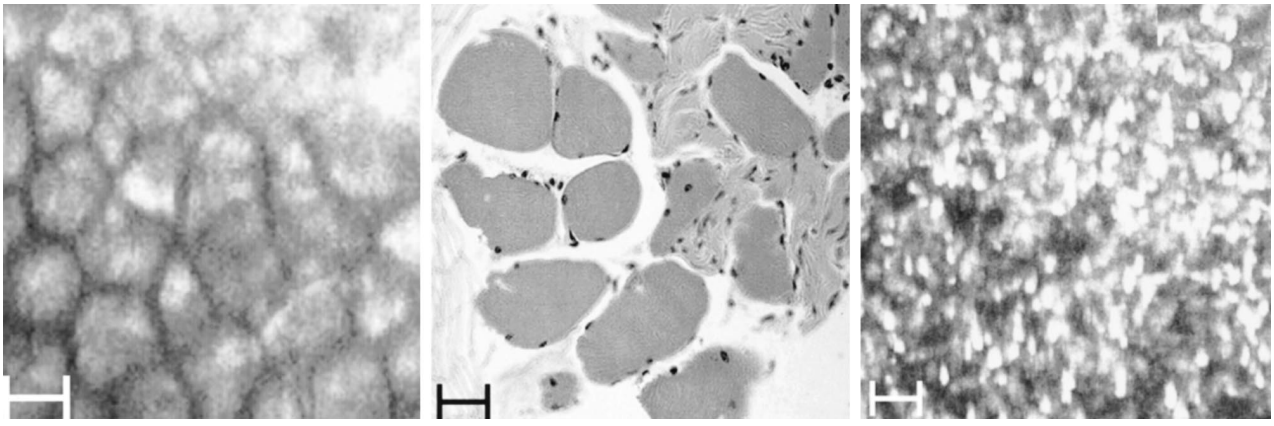

Fig. 3. (*Left*) TPCM on day 0. Muscle fibers are visualized based on NAD(P)H fluorescence from the myocytes (original magnification, ×40; x-y section 12.5 μm deep from wound bed); scale bar, 11 μm. (*Center*) Light microscopy on day 0. Muscle fibers (hematoxylin and eosin; original magnification, ×40; en face section 10 μm deep from base of dermis); scale bar, 11 μm. (*Right*) TPCM on day 0. Muscle fibers (DNA stain; original magnification, ×40; x-y section 10 μm deep).

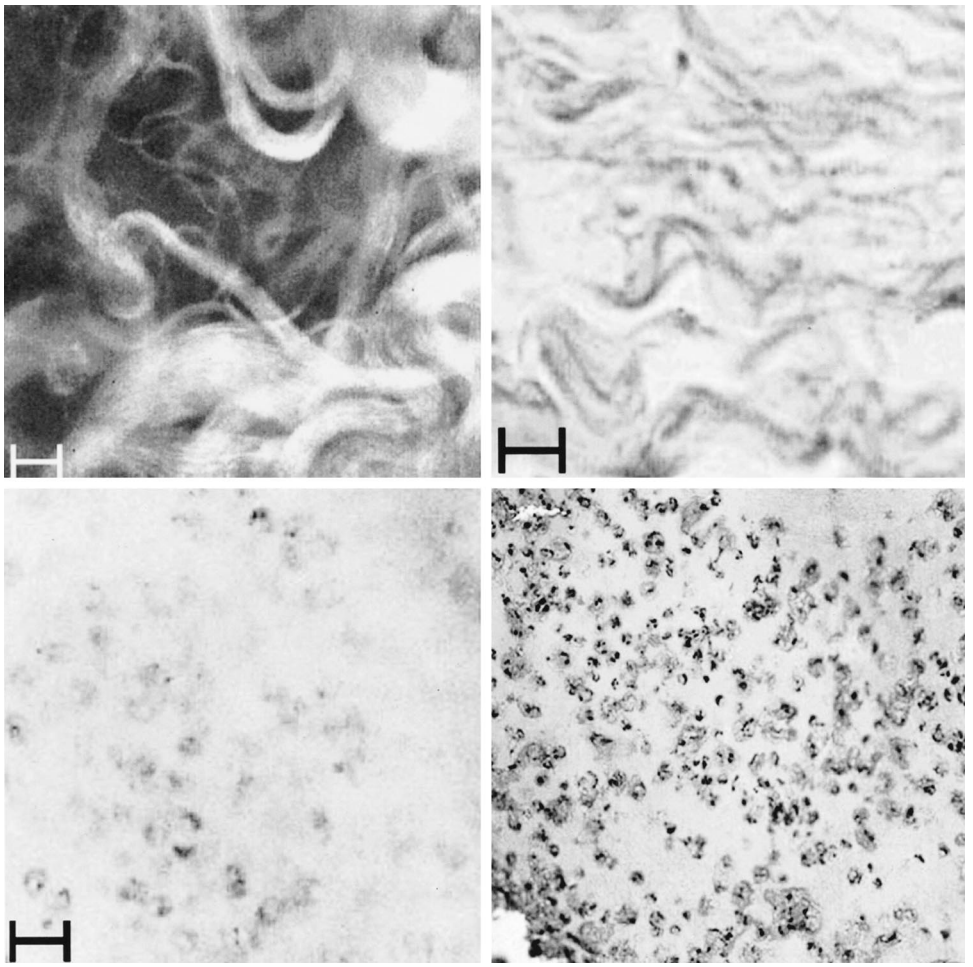

FIG. 4. (*Above*, *left*) TPCM on day 3. Fascia fibers (original magnification, ×40; x-y section 7.5 μm deep from wound surface); scale bar, 11 μm. (*Above*, *right*) Light microscopy on day 3. Fascia fibers (hematoxylin and eosin; original magnification, ×40; en face section 7.5 μm deep to the wound surface); scale bar, 11 μm. (*Below*, *left*) TPCM on day 3; inflammatory cells (original magnification, ×40; x-y section near wound surface); scale bar, 11 μm. (*Below*, *right*) Light microscopy on day 3. Inflammatory cells (hematoxylin and eosin; original magnification, ×40; en face section near wound surface).

Day 28 images depict a continued closed and epithelialized wound. The fluorescence of the basal cells is very intense. Many of the TPCM images are obscured by hair shafts (Fig. 7, *left*), 60 μm deep into the skin surface. These hair shafts are likely ingrowths from the surrounding normal tissue. A comparative light microscopy section (Fig. 7, *right*), 70 μm into the wound bed, shows a better defined hair follicle line and epithelial cells. It is theoretically possible with TPCM to obtain a three-dimensional reconstruction of structures such as hair follicles.

DISCUSSION

TPCM allows the potential for nondestructive testing of healing wounds. Full-thickness defects began to heal by an initial inflammatory reaction along with collagen gel deposition. This was followed by maturation of the collagen gel into fibrils, and later into thick, mature fibers. Later in the wound-healing process, a migrating tongue of epithelium could be seen advancing across the wound. The prolonged inflammatory stage and the delay in the epithelialization were attributable mainly to the full-thickness nature of the skin defect. This technology might be particularly appropriate for studying wound-healing events such as inflammation, collagen structure, and angiogenesis.

This nondestructive technology will undoubtedly have applications in other areas of skin abnormalities, including skin malignan-

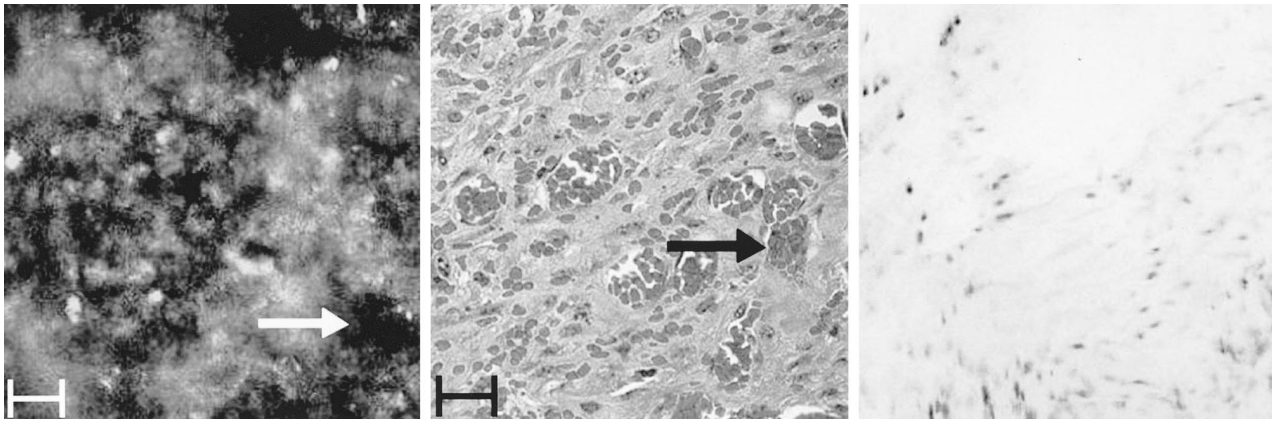

FIG. 5. (*Left*) TPCM on day 10. New blood vessels and collagen fibers; *arrow* points to presumed new blood vessel (hematoxylin and eosin; original magnification, ×40; x-y section, 15 μm deep from wound surface); scale bar, 11 μm. (*Center*) Light microscopy on day 10. New blood vessels and collagen fibers; *arrow* points to new blood vessel (hematoxylin and eosin; original magnification, ×40; en face section 15 μm deep from wound surface); scale bar, 11 μm. (*Right*) TPCM on day 7. Collagen fibers (DNA stain; original magnification, ×40; x-y section superficial layers 5 μm deep).

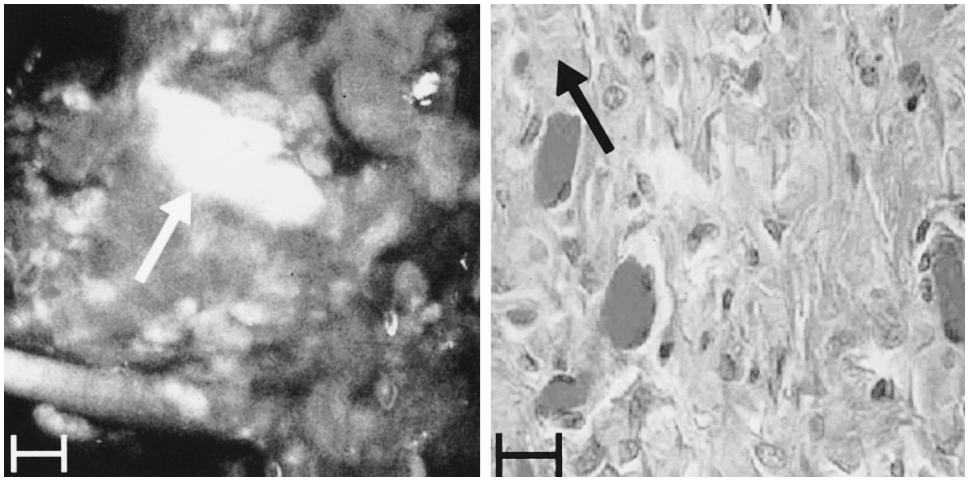

FIG. 6. (*Left*) TPCM day 14. Collagen fibers; *arrow* points to presumed collagen bundle (original magnification, ×40; x-y section 17 μm deep from wound surface); scale bar, 11 μm. (*Right*) Light microscopy on day 14. Collagen fibers; *arrow* points to collagen bundle (hematoxylin and eosin; original magnification, ×40; en face section, 17 μm deep from wound surface); scale bar, 11 μm.

cies and inflammatory disorders. It is conceivable that the need for an invasive biopsy may be eliminated in some cases.

This technique is highly sensitive to movement. Our best images were obtained from animals that had been euthanized, where respiratory movement was eliminated. Further development including the use of image-stabilizing lenses or a microscope stage and increasing the scanning rate will possibly reduce this problem.

The maximum penetration depth of two-photon microscopy in tissues is still a very active research topic.[9–13] The imaging depth depends on a number of factors. Exponential signal attenuation caused by scattering and absorption is a major effect.[14] The degradation in excitation efficiency caused by pulse broadening also must be considered.[15] Furthermore, there may also be resolution degradation because of index of refraction variations and multiple scattering effects in tissues.[16] Operationally, although imaging depth on the order of 0.5 mm has been achieved using exogenous fluorescent probes,[17] the imaging depth in living tissue based on endogenous fluorescence of ultraviolet chromophores such as NAD(P)H and elastin has been found to be approximately 200 μm.[18] Within this range, there is no significant resolution loss, and image contrast

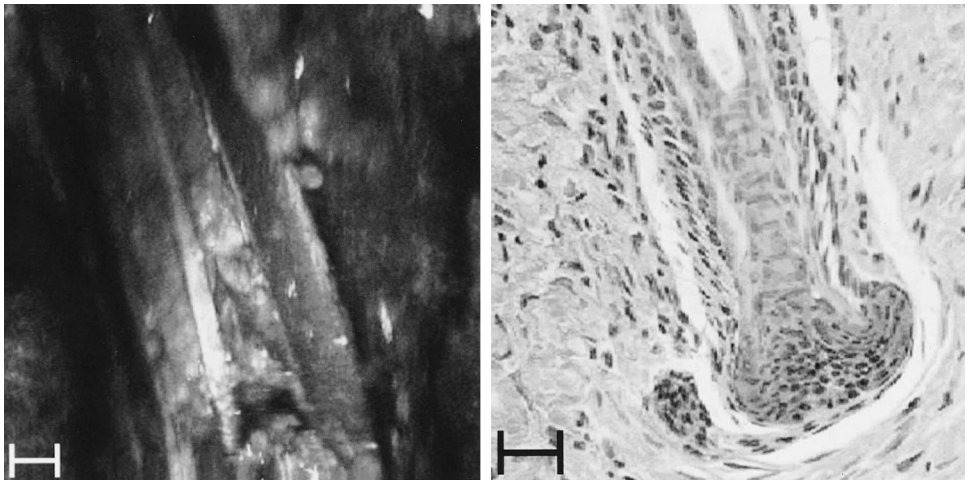

FIG. 7. (*Left*) TPCM on day 28. Hair follicle (original magnification, ×40; x-y section, 60 μm depth from skin surface); scale bar, 11 μm. (*Right*) Light microscopy on day 28. Hair follicle (hematoxylin and eosin; original magnification, ×40; en face histology, 70 μm depth from skin surface); scale bar, 11 μm.

remains acceptable. In this work, the imaging depth is on the order of 100 μm from the tissue surface.

Methods to improve image resolution and clarity are being tested. Studies have shown that the addition of cyanide to the tissue being visualized alters the NADP:NAD(P)H ratio.[18,19] This in turn increases the fluorescence of the tissue, which improves the resolution. Decreasing the distance between the *z*-planes may also result in better cross-sectional images, which may be easier to compare with conventional microscopy.

TPCM images have *x*-, *y*-, and *z*-plane resolution, providing the advantage of three-dimensional visualization. The current microscope yields a cubic array of 256 pixels per plane. The lateral and axial resolution for TPCM using 780-nm excitation is 0.5 and 0.7 μm/pixel, respectively. The lateral resolution for light microscopy is approximately 0.3 μm.

As most investigators are most familiar with transverse sections, additional studies will be required to gain familiarity with this en face methodology. Alternatively, improvements in TPCM microscopy technology could potentially improve visualization in the transverse plane. Using three-dimensional analytic techniques, additional anatomic data may be obtained using TPCM. Although two-photon confocal microscopy currently provides lower resolution than conventional histology, this study demonstrates successful imaging of the wound-healing process over a period of 28 days. With this technology, three-dimensional structural characteristics can be obtained sequentially in a nondestructive manner. This may improve our understanding of the crucial steps in inflammation, scar formation, and future diagnosis of skin diseases.

Dennis P. Orgill, M.D., Ph.D.
Division of Plastic and Reconstructive Surgery
Brigham and Women's Hospital
75 Francis Street
Boston, Mass. 02115
dorgill@partners.org

ACKNOWLEDGMENT

We thank Jennifer Neuwalder for careful review of the manuscript.

REFERENCES

1. Chance, B., and Thorell, B. Localization and kinetics of reduced pyridine nucleotide in living cells by microfluorometry. *J. Biol. Chem.* 234: 3044, 1959.
2. Thomas, J., Elsden, D. F., and Partridge, S. M. Degradation products from elastin. *Nature* 200: 651, 1963.
3. La Bella, F. S., and Lindsay, W. G. The structure of human aortic elastin as influence by age. *J. Gerontol.* 18: 111, 1963.
4. La Bella, F. S., and Gerald, P. Structure of collagen from human tendon as influence as influence by age and sex. *J. Gerontol.* 20: 54, 1965.
5. Agarwal, A., Coleno, M. L., Wallace, V. P., et al. Two-photon laser scanning microscopy of epithelial cell-modulated collagen density in engineered human lung tissue. *Tissue Eng.* 7: 191, 2001.
6. Campagnola, P. J., Clark, H. A., Mohler, W. A., Lewis, A., and Loew, L. M. Second-harmonic imaging microscopy of living cells. *J. Biomed. Optics* 6: 277, 2001.
7. Master, B. A., and Thaer, A. A. Real-time scanning slit confocal microscopy of the in vivo human cornea. *Appl. Optics* 33: 695, 1994.
8. Navarro, F. A., So, P. T. C., Oriessen, A., et al. Two

photon confocal microscopy in wound healing. *Prog. Biomed. Optics Imaging* 19: 27, 2001.
9. Blanca, C. M., and Saloma, C. Monte Carlo analysis of two-photon fluorescence imaging through a scattering medium biological microstructures applications. *Appl. Optics* 37: 8092, 1998.
10. Centonze, V. E., and White, J. G. Multiphoton excitation provides optical sections from deeper within scattering specimens than confocal imaging. *Biophys. J.* 75: 2015, 1998.
11. DeGraw, G. J., Vroom, J. M., Van der Voort, H. T. M., and Gerritsen, H. C. Imaging properties in two-photon excitation microscopy and effects of refractive-index mismatch in thick specimens. *Appl. Optics* 38: 5995, 1999.
12. Daria, V., Blanca, C. M., Nakamura, O., Kawata, S., and Saloma, C. Image contrast enhancement for two photon fluorescence microscopy in a turbid medium. *Appl. Optics* 37: 7960, 1998.
13. Gerritsen, H. C., and de Graw, C. J. Imaging of optically thick specimen using two-photon excitation microscopy. *Microsc. Res. Tech.* 47: 206, 1999.
14. Dunn, A. K., Wallace, V. P., Coleno, M., Berns, M. W., and Tromberg, B. J. Influence of optical properties on two-photon fluorescence imaging in turbid samples. *Appl. Optics* 39: 1194, 2000.
15. Blanca, C. M., and Saloma, C. Efficient analysis of temporal broadening of a pulsed focused gaussian beam in scattering media. *Appl. Optics* 38: 5433, 1999.
16. Schilders, S. P., and Gu, M. Limiting factors on image quality in imaging through turbid media under single-photon and two-photon excitation. *Microsc. Microanal.* 6: 156, 2000.
17. Kleinfeld, D., Mitra, P. P., Helmchen, F., and Denk, W. Fluctuations and stimulus-induced changes in blood flow observed in individual capillaries in layers 2 through 4 of rat neocortex. *Proc. Natl. Acad. Sci. U.S.A.* 95: 15741, 1998.
18. Master, B. R., So, P. T. C., and Grantton, E. Multiphoton excitation fluorescence microscopy and spectroscopy of in vivo human skin. *Biophys. J.* 72: 2405, 1997.
19. Piston, D. W., Masters, B. R., and Webb, W. W. Three-dimensionally resolved NAD(P)H cellular metabolic redox imaging of the in situ cornea with two-photon excitation laser scanning microscopy. *J. Microsc.* 178: 20, 1995.